# Design, Synthesis, and In Vitro, In Silico and In Cellulo Evaluation of New Pyrimidine and Pyridine Amide and Carbamate Derivatives as Multi-Functional Cholinesterase Inhibitors

**Martina Bortolami [1], Fabiana Pandolfi [1], Valeria Tudino [2], Antonella Messore [2], Valentina Noemi Madia [2], Daniela De Vita [3], Roberto Di Santo [2,4], Roberta Costi [2,4], Isabella Romeo [5,6], Stefano Alcaro [5,6,*], Marisa Colone [7], Annarita Stringaro [7], Alba Espargaró [8,9], Raimon Sabatè [8,9] and Luigi Scipione [2,*]**

[1] Department of Scienze di Base e Applicate per l'Ingegneria, Sapienza University of Rome, Via Castro Laurenziano 7, 00185 Rome, Italy; martina.bortolami@uniroma1.it (M.B.); fabiana.pandolfi@uniroma1.it (F.P.)
[2] Department of Chimica e Tecnologia del Farmaco, Sapienza University of Rome, Piazzale Aldo Moro 5, 00185 Rome, Italy; valeria.tudino@uniroma1.it (V.T.); antonella.messore@uniroma1.it (A.M.); valentinanoemi.madia@uniroma1.it (V.N.M.)
[3] Department of Environmental Biology, Sapienza University of Rome, Piazzale Aldo Moro 5, 00185 Rome, Italy; daniela.devita@uniroma1.it
[4] Instituto Pasteur, Fondazione Cenci Bolognetti, Sapienza University of Rome, Piazzale Aldo Moro 5, 00185 Rome, Italy; roberto.disanto@uniroma1.it (R.D.S.); roberta.costi@uniroma1.it (R.C.)
[5] Net4Science Academic Spin-Off, Università degli Studi "Magna Græcia" di Catanzaro, Campus "S. Venuta", Viale Europa, 88100 Catanzaro, Italy;
[6] Dipartimento di Scienze della Salute, Università degli Studi "Magna Græcia" di Catanzaro, 88100 Catanzaro, Italy; isabella.romeo@unicz.it
[7] National Center for Drug Research and Evaluation, Istituto Superiore di Sanità, 00161 Rome, Italy; marisa.colone@iss.it (M.C.); annarita.stringaro@iss.it (A.S.)
[8] Department of Pharmacy and Pharmaceutical Technology and Physical-Chemistry, Faculty of Pharmacy and Food Sciences, University of Barcelona, 27-31 Barcelona, Catalonia, Spain ;
[9] Institute of Nanoscience and Nanotechnology (IN$^2$UB), 08028 Barcelona, Spain; aespargaro@ub.edu (A.E.); rsabate@ub.edu (R.S.)
* Correspondence: alcaro@unicz.it (SA); luigi.scipione@uniroma1.it (LS).

## SUPPORTING INFORMATION

**Dixon's plot of compounds 12 and 14 towards *eq*BChE** pag. 2

**$IC_{50}$ graph of compound 18 towards *eq*BChE** pag. 3

***In silico* studies** pag. 4

**UV-Vis titration spectra and Job's plots for selected compounds** pag. 7

## Dixon's plot of compounds 12 and 14 towards *eq*BChE

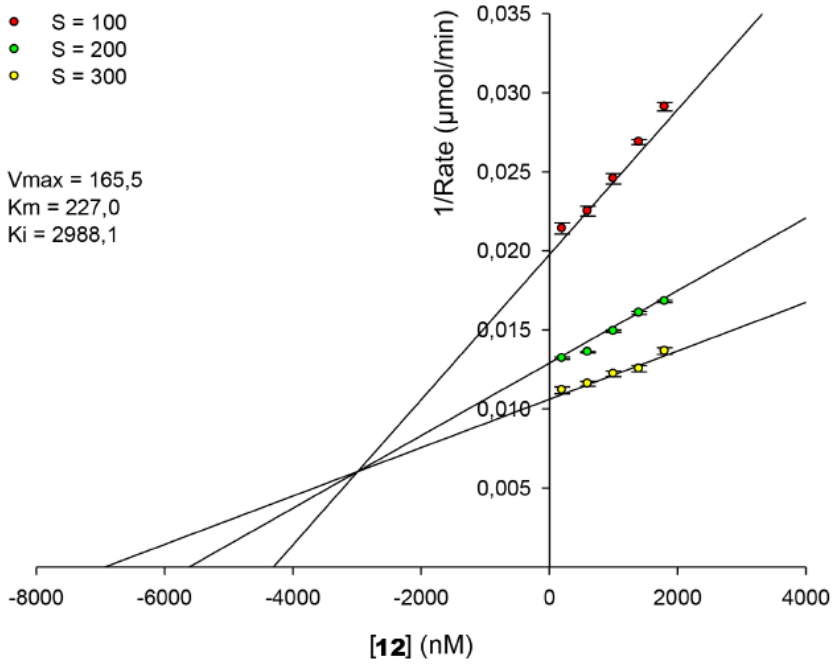



**Figure S1.** Dixon's plot obtained for **12** (200-1800 nM), in presence of *eq*BChE (0.0833 U/mL) and ASCh (100-300 µM). Competitive inhibition mechanism was observed (Ki = 2.988 ± 0.190 µM, $R^2$ = 0.987).

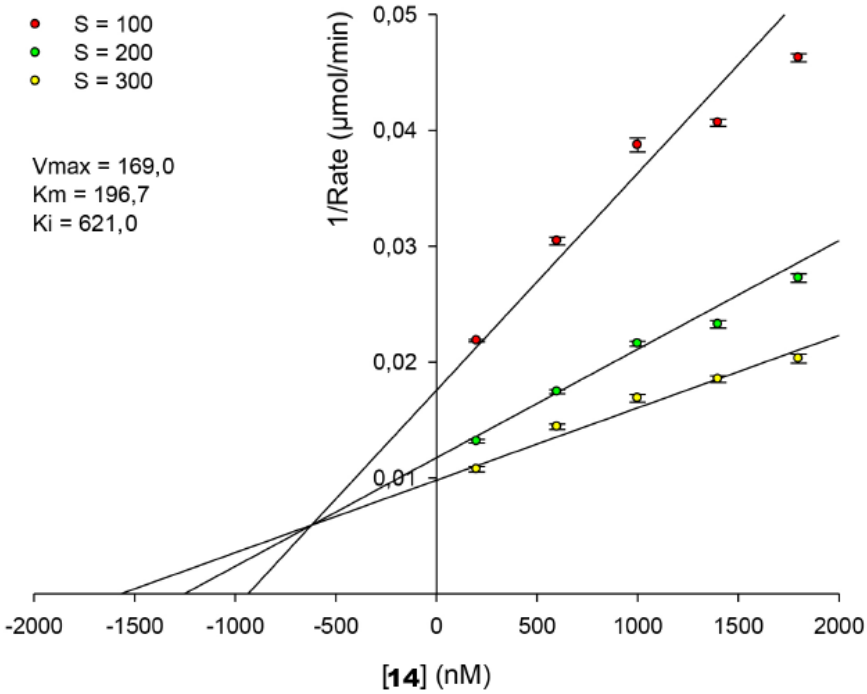



**Figure S2.** Dixon's plot obtained for **14** (200-1800 nM), in presence of *eq*BChE (0.0833 U/mL) and ASCh (100-300 µM). Competitive inhibition mechanism was observed (Ki = 0.621 ± 0.043 µM, $R^2$ = 0.980).

## $IC_{50}$ graph of compound 18 towards *eq*BChE

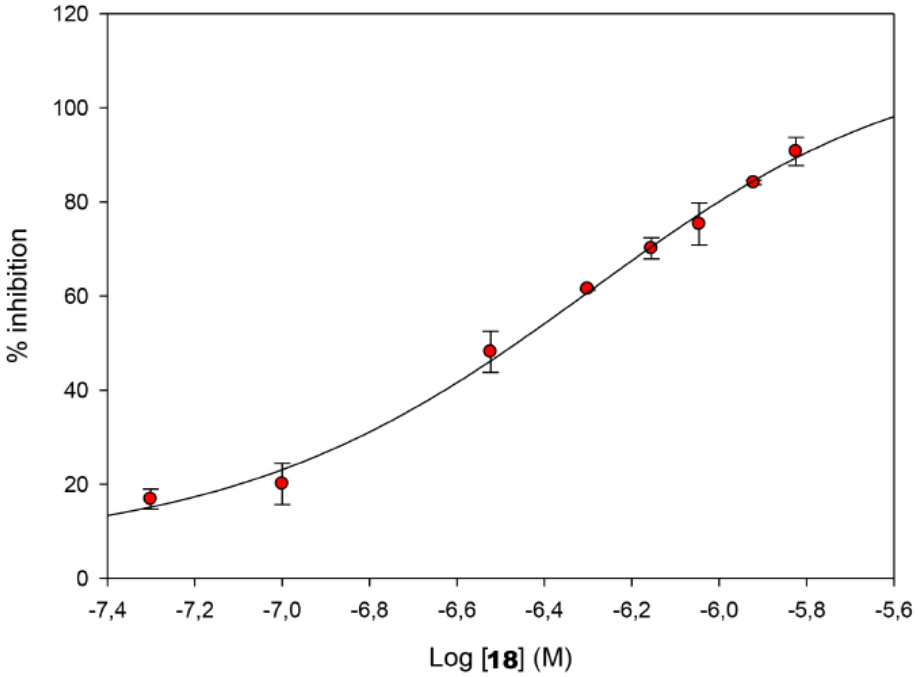



**Figure S3.** $IC_{50}$ graph for compound **18** (50-1500 nM), in presence of *eq*BChE (0.0833 U/mL) and ASCh (100 μM). The $IC_{50}$ value extrapolated from the graph is 454 ± 82 nM.

## *In silico* studies

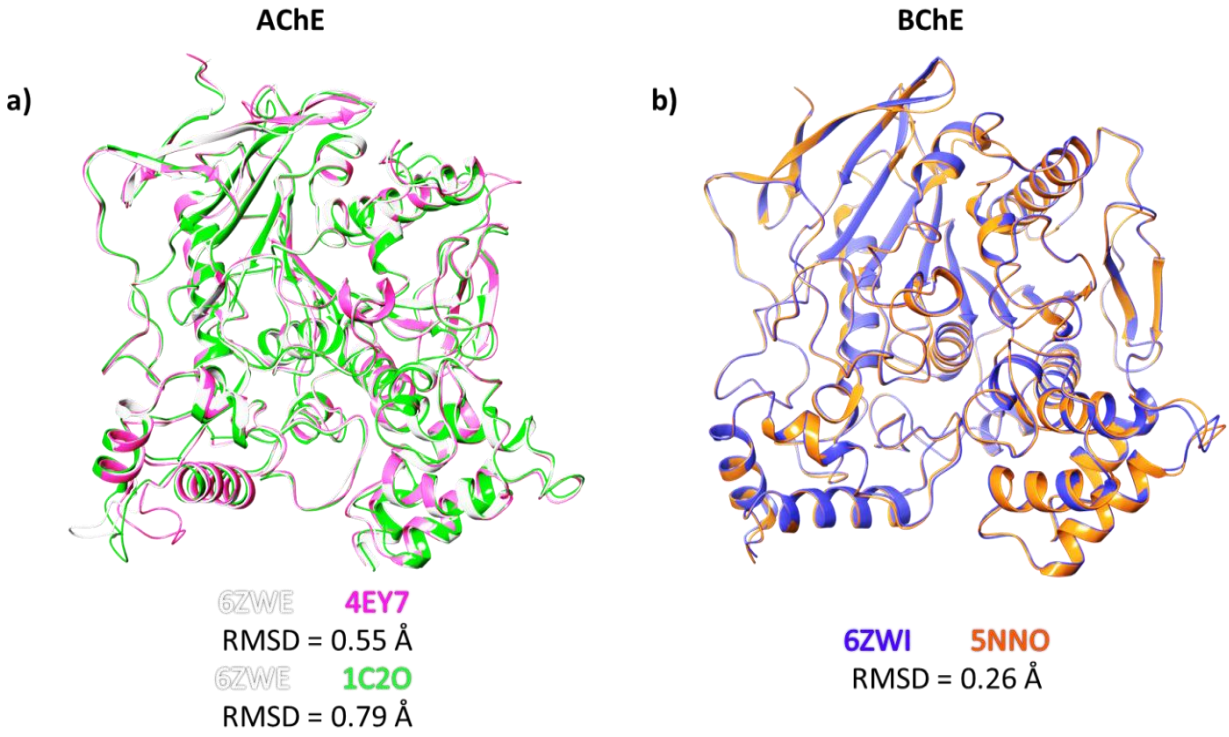



**Figure S4. a)** Superposition of *Electrophorus electricus* AChE (PDB code: 1C2O) and human AChE (PDB code: 4EY7) with human AChE (PDB code: 6ZWE) and **b)** superposition of human BChE (PDB code: 5NN0) and human BChE (PDB code: 6ZWI) generated by Protein Structure Alignment.

```
                                                
```

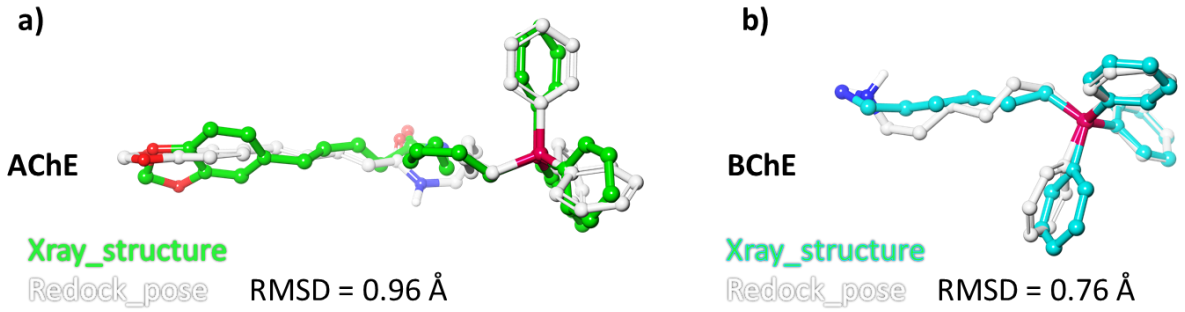



**Figure S6.** Superimposition of the re-docked pose (gray carbons) and co-crystallized ligand of **a)** *h*AChE and **b)** *h*BChE receptors, represented, respectively, in green and blue carbons. RMSD was found to be 0.96 Å for *h*AChE ligand and 0.76 Å for *h*BChE ligand.

**Table S1.** GlideScore values (Kcal/mol) of compounds **3-19** for binding *h*AChE and *h*BChE and re-docking values of co-crystallized ligands of 6ZWE and 6ZWI PDB structures.

| **Compound** | | **GlideScore (Kcal/mol)** | |
|---|---|---|---|
| | | ***h*AChE** | ***h*BChE** |
| **Pyrimidine amide derivatives** | **3** | -6.37 | -6.61 |
| | **4** | -7.87 | -7.31 |
| | **5** | -8.02 | -7.81 |
| | **6** | -8.04 | -7.78 |
| | **7** | -7.68 | -7.82 |
| | **8** | -7.87 | -7.76 |
| | **9** | -8.07 | -7.55 |
| | **10** | -6.18 | -5.54 |
| | **11** | -8.77 | -8.24 |
| **Pyridine amide derivatives** | **12** | -6.38 | -6.68 |
| | **13** | -8.23 | -7.67 |
| | **14** | -8.05 | -8.13 |
| | **15** | -8.22 | -8.46 |
| **Carbamate derivatives** | **16** | -7.31 | -7.90 |
| | **17** | -7.31 | -7.10 |
| | **18** | -7.59 | -8.49 |
| | **19** | -7.65 | -7.67 |
| **X-ray ligand** | **6ZWE** | -10.78 | - |
| | **6ZWI** | - | -7.71 |

**Table S2**. Molecular Surface Area (Å$^3$) of the best docking poses of the **3-19** compounds into AChE and BChE binding pocket.

| Compound | Molecular Surface Area (Å$^3$) | |
|---|---|---|
| | AChE | BChE |
| **3** | 313.06 | 320.23 |
| **4** | 332.09 | 341.92 |
| **5** | 414.72 | 429.86 |
| **6** | 343.74 | 354.38 |
| **7** | 338.51 | 342.67 |
| **8** | 334.57 | 343.06 |
| **9** | 337.76 | 348.65 |
| **10** | 317.98 | 319.84 |
| **11** | 343.61 | 356.03 |
| **12** | 316.54 | 335.67 |
| **13** | 341.36 | 346.47 |
| **14** | 409.92 | 436.15 |
| **15** | 332.62 | 359.54 |
| **16** | 320.26 | 333.34 |
| **17** | 349.98 | 356.32 |
| **18** | 335.73 | 336.52 |
| **19** | 341.99 | 359.64 |
| **Average value** | 342.56 | 354.13 |

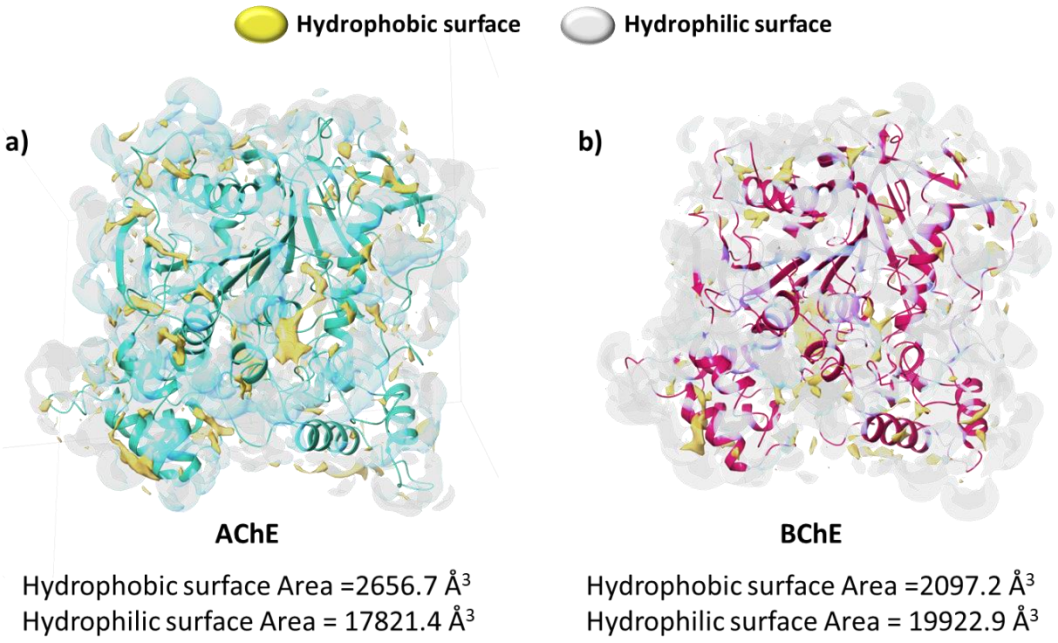



**Figure S7**. Views of Hydrophobic and Hydrophilic surface area in yellow and grey solid surface, respectively, of **a)** *h*AChE (turquoise cartoon) and **b)** *h*BChE receptors (pink cartoon).

## UV-Vis titration spectra and Job's plots for selected compounds

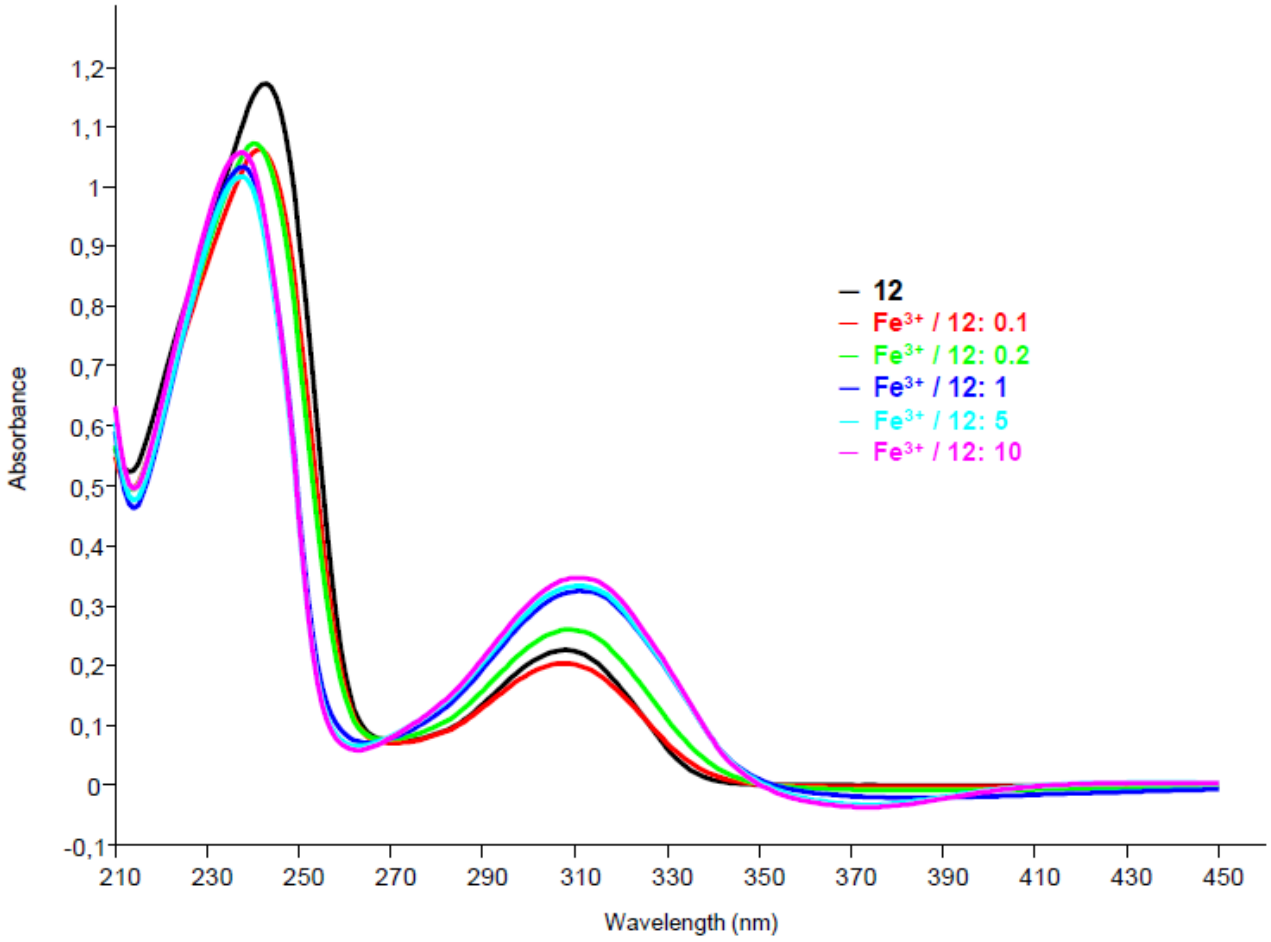



**Figure S8.** UV-Vis titration of ligand **12** with $Fe^{3+}$. The greatest variations in spectra with increasing amount of metal are observed at 251 nm, with a reduction of absorbance, and at 320 nm, with an increase of absorbance. There are two isosbestic points at 267 and 350 nm.

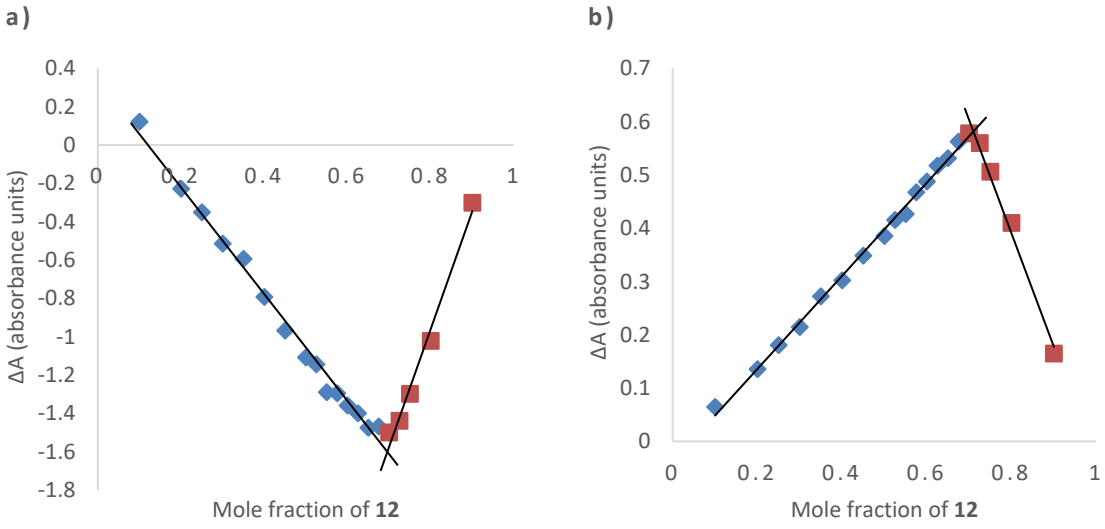



**Figure S9.** Job's plot of compound **12** in presence of $Fe^{3+}$: variation of the absorbance (ΔA) at the wavelength of 251 nm in **a)** or at 320 nm in **b)**, in ordinate, versus the mole fraction of **12**, in abscissa. X (mole fraction that causes the maximum variation of absorbance) = 0.69 in **a)**, 0.71 in **b)**; n (number of ligand molecules per cation) = 2.

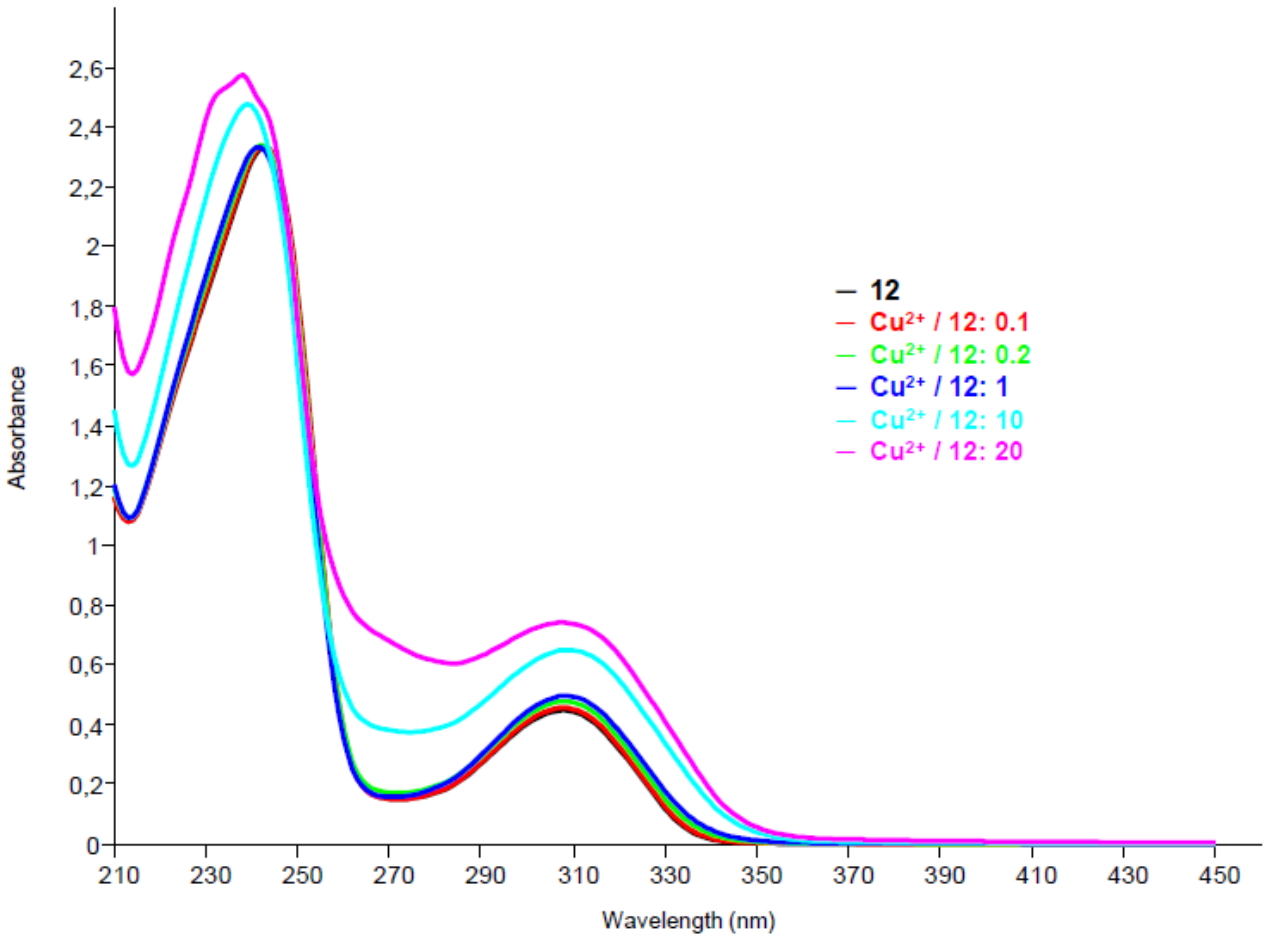



**Figure S10.** UV-Vis titration of ligand **12** with $Cu^{2+}$. The greatest variations in spectra with increasing amount of metal are observed at 235, 270 and 310 nm, with an increase of absorbance.

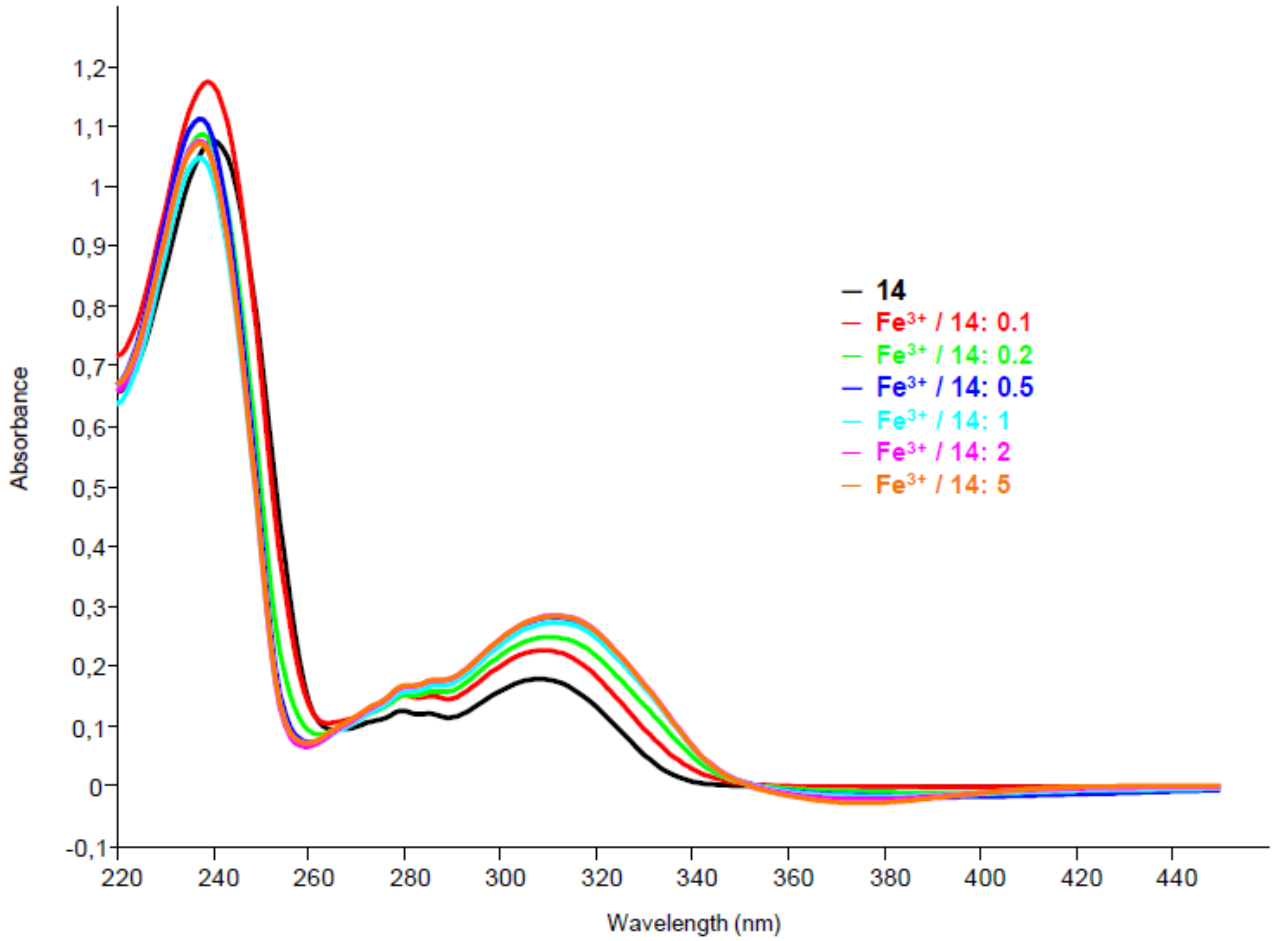



**Figure S11.** UV-Vis titration of ligand **14** with $Fe^{3+}$. The greatest variation in spectra with increasing amount of metal is observed at 310 nm, with an increase of absorbance. There are two isosbestic points at 266 and 350 nm.

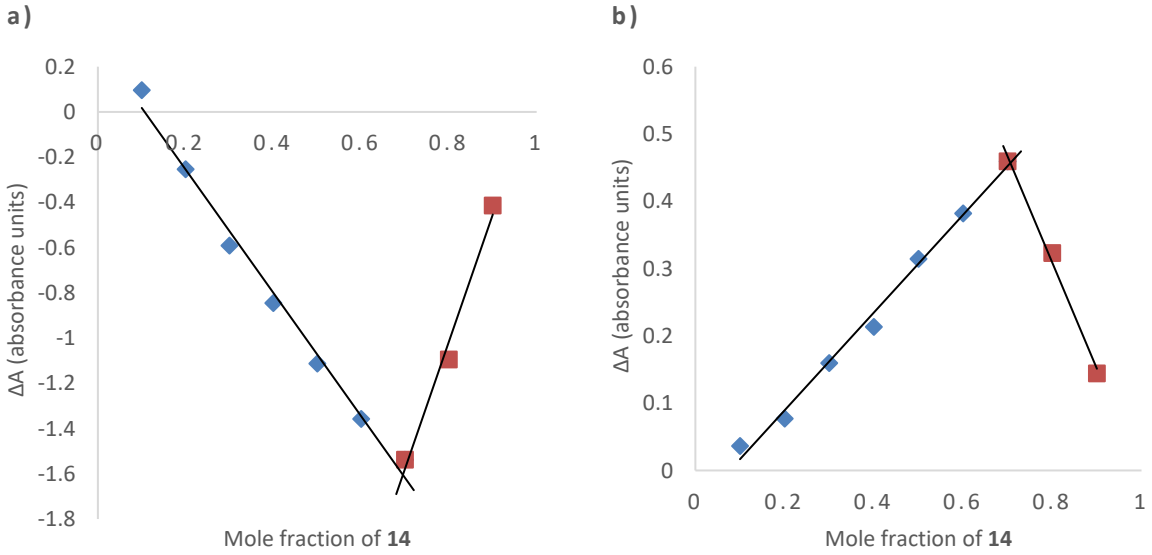



**Figure S12.** Job's plot of compound **14** in presence of $Fe^{3+}$: variation of the absorbance (ΔA) at the wavelength of 250 nm in **a)** or at 310 nm in **b)**, in ordinate, versus the mole fraction of **14**, in abscissa. X (mole fraction that causes the maximum variation of absorbance) = 0.70 in **a)**, 0.71 in **b)**; n (number of ligand molecules per cation) = 2.

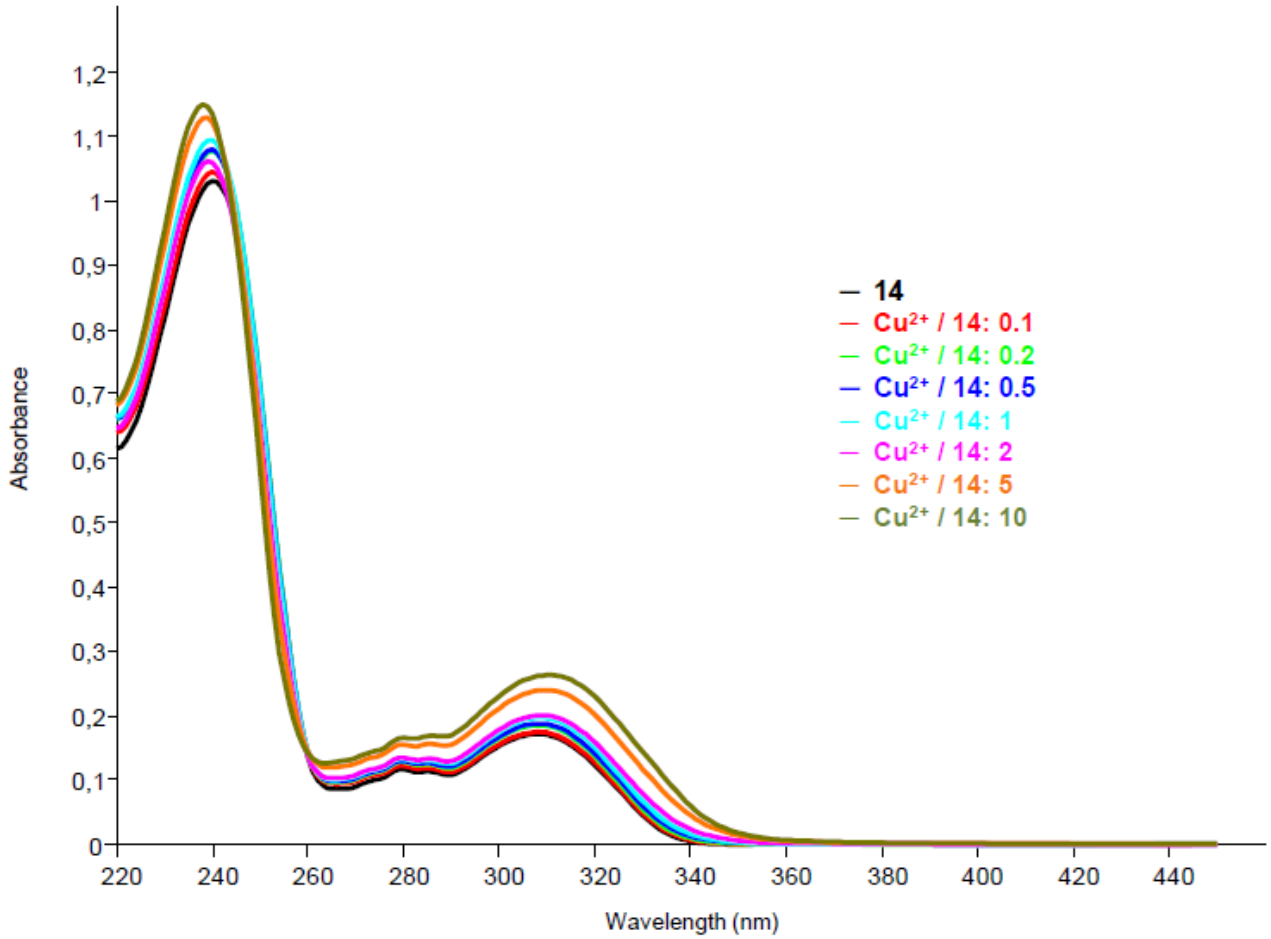



**Figure S13.** UV-Vis titration of ligand **14** with $Cu^{2+}$. The greatest variation in spectra with increasing amount of metal is observed at 310 nm, with an increase of absorbance. There is an isosbestic point at 260 nm.

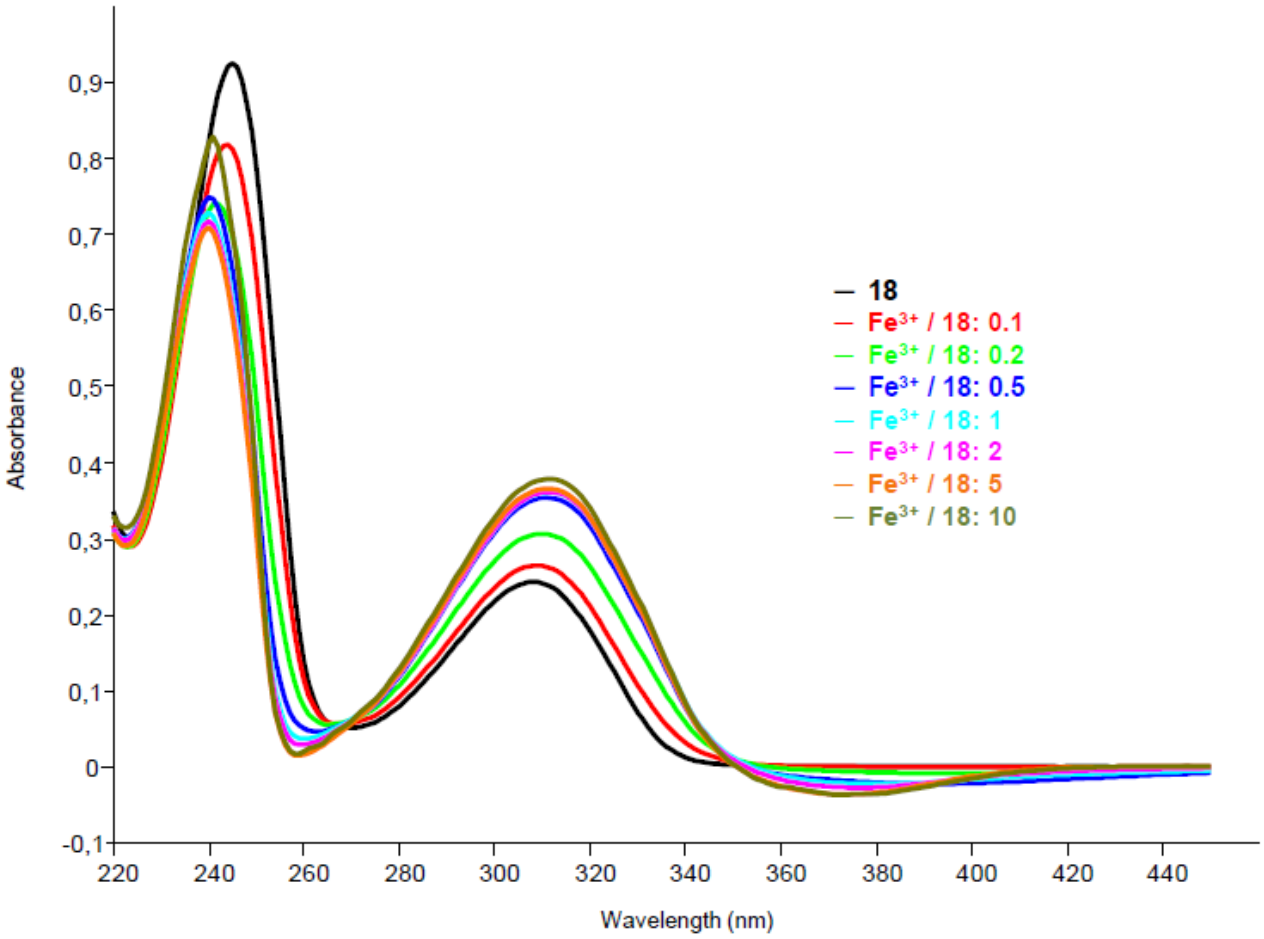



**Figure S14.** UV-Vis titration of ligand **18** with $Fe^{3+}$. The greatest variations in spectra with increasing amount of metal are observed at 245 nm, with a reduction of absorbance, and at 310 nm, with an increase of absorbance. There are two isosbestic points at 267 and 353 nm.

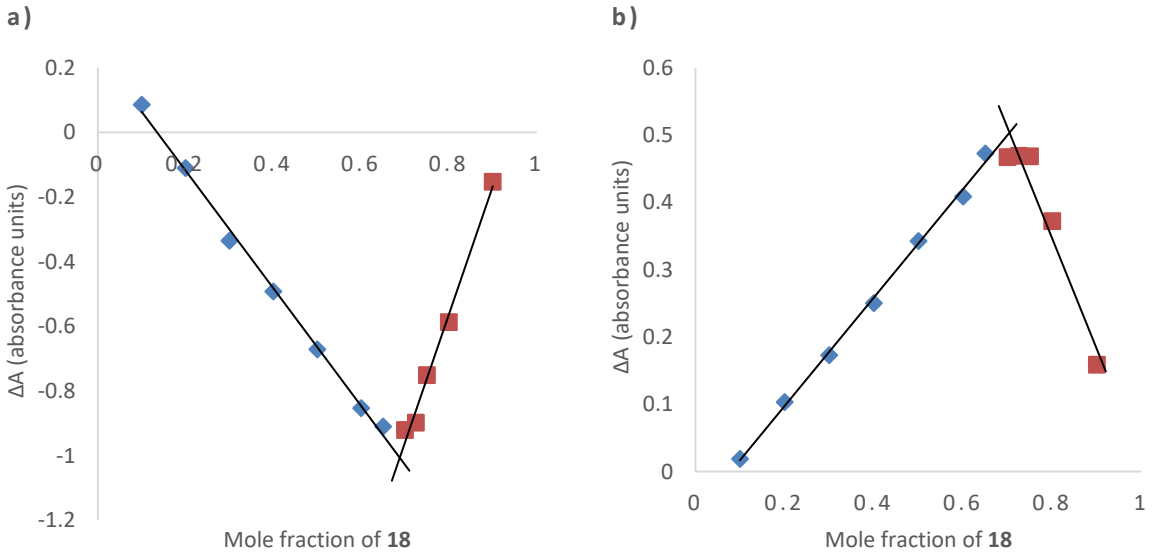



**Figure S15.** Job's plot of compound **18** in presence of $Fe^{3+}$: variation of the absorbance (ΔA) at the wavelength of 245 nm in **a)** or at 310 nm in **b)**, in ordinate, versus the mole fraction of **18**, in abscissa. X (mole fraction that causes the maximum variation of absorbance) = 0.69 in **a)**, 0.70 in **b)**; n (number of ligand molecules per cation) = 2.

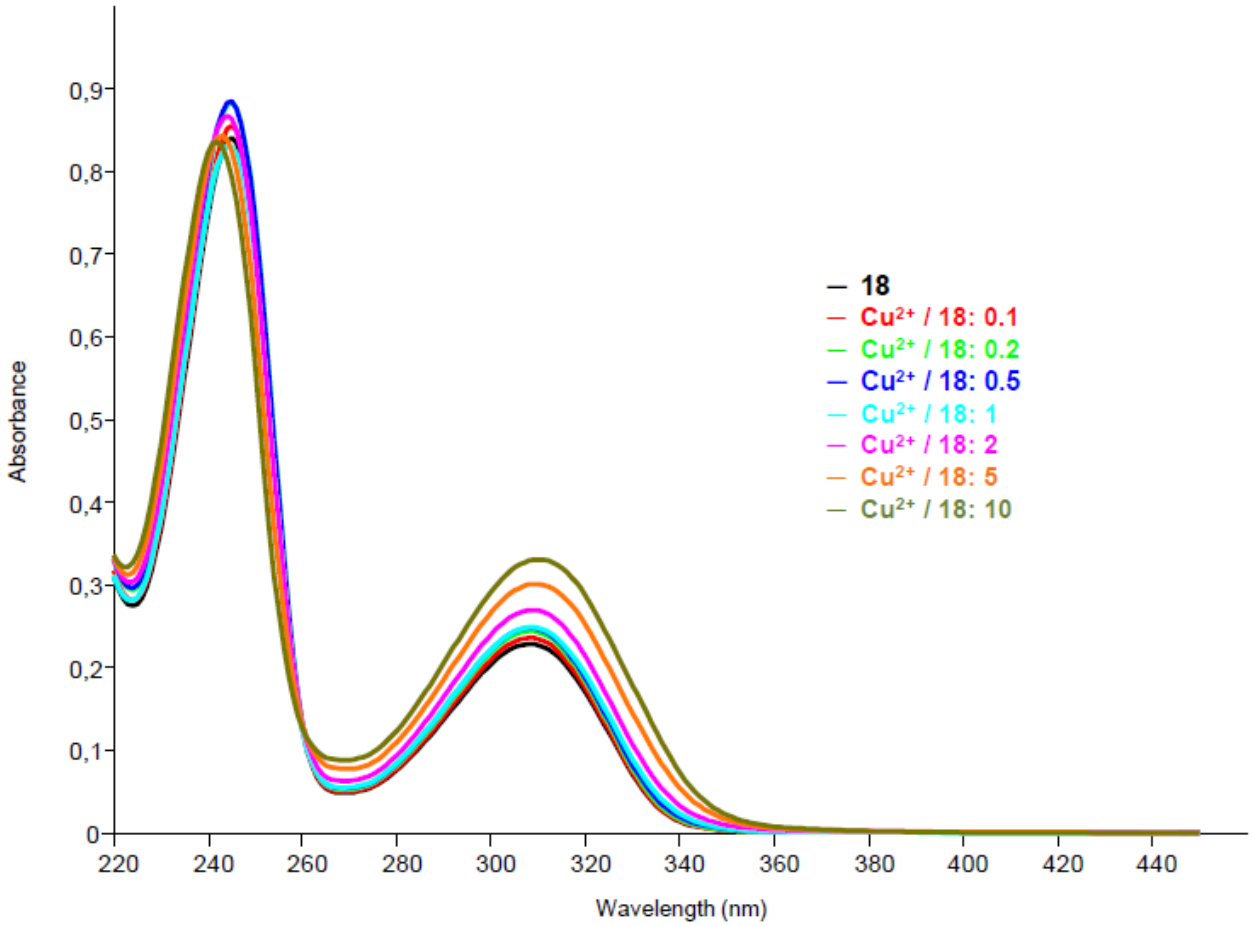



**Figure S16.** UV-Vis titration of ligand **18** with $Cu^{2+}$. The greatest variations in spectra with increasing amount of metal are observed at 270 and 310 nm, with an increase of absorbance. There is an isosbestic point at 261 nm.

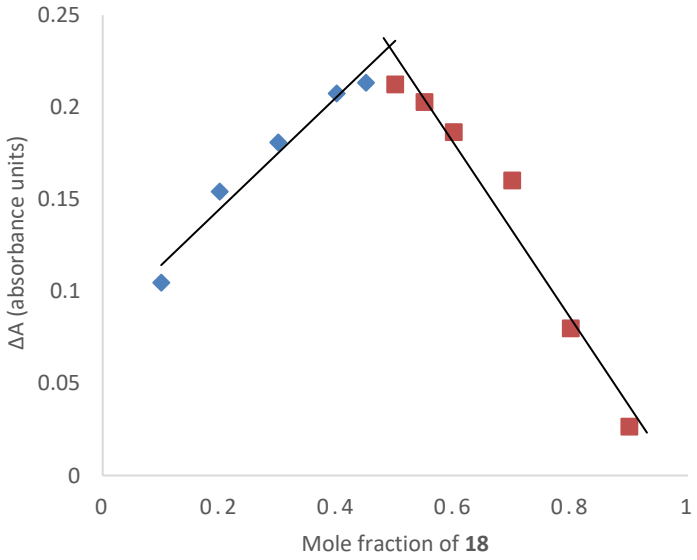



**Figure S17.** Job's plot of compound **18** in presence of $Cu^{2+}$: variation of the absorbance (ΔA) at the wavelength of 330 nm, in ordinate, versus the mole fraction of **18**, in abscissa. X (mole fraction that causes the maximum variation of absorbance) = 0.49; n (number of ligand molecules per cation) = 1.